

Biophysical inference of epistasis and the effects of mutations on protein stability and function

Jakub Otwinowski

University of Pennsylvania, Biology Department, jakubo@sas.upenn.edu

Abstract

Understanding the relationship between protein sequence, function, and stability is a fundamental problem in biology. While high-throughput methods have produced large numbers of sequence-function pairs, functional assays do not distinguish whether mutations directly affect function or are destabilizing the protein. Here, we introduce a statistical method to infer the underlying biophysics from a high-throughput binding assay by combining information from many mutated variants. We fit a thermodynamic model describing the bound, unbound, and unfolded states to high quality data of protein G domain B1 binding to IgG-Fc. We infer an energy landscape with distinct folding and binding energies for each substitution providing a detailed view of how mutations affect binding and stability across the protein. We accurately infer folding energy of each variant in physical units, validated by independent data, whereas previous high-throughput methods could only measure indirect changes in stability. While we assume an additive sequence-energy relationship, the binding fraction is epistatic due its non-linear relation to energy. Despite having no epistasis in energy, our model explains much of the observed epistasis in binding fraction, with the remaining epistasis identifying conformationally dynamic regions.

Author Summary

Determining how mutations impact protein stability and function is instrumental in understanding how proteins carry out their biological tasks, how they evolve, and how to engineer novel proteins. However measuring differences in function between mutated variants does not distinguish whether mutations are directly affecting function or are destabilizing the protein. Here, we fit a thermodynamic model to data describing how thousands of variants of a protein bind to an antibody fragment. We accurately infer separate folding and binding energies in physical units, providing a detailed energy landscape describing how mutations affect binding and stability across the protein, and our non-linear model reproduces many of the observed interactions between sites.

Introduction

Deep mutational scanning (DMS) studies have produced detailed maps of how proteins and regulatory sequences are related to function by assaying up to millions of mutated variants, and has had many applications, from identifying viral epitopes to protein engineering [1, 2]. While these studies aim to understand molecular function and evolution by collecting large numbers of sequence-function pairs, the full sequence-function map

is very difficult to determine due to the enormity of sequence space. Different sites in a sequence may not contribute to molecular function independently, and the effect of a substitution at one site may depend on the genetic background. This non-additivity, or epistasis, means that the entire space of possible sequences may have to be explored to understand molecular function.

Given the limited data, mathematical modeling is necessary to make any progress. However, purely statistical inferences are difficult to interpret in terms of known biology, and can be too flexible to make reliable predictions [3, 4]. On the other hand, biophysical systems are not arbitrarily complex as they follow physical laws and structural constraints. In other words, there is hope that biophysical knowledge can help explain sequence-function relationships. A powerful assumption is that in between sequence and function lie relevant intermediate phenotypes for which we can derive relatively simple relations to sequence and function [5].

The stability of a protein’s fold is a fundamental molecular phenotype under selection. Studying how mutations affect stability is a fundamental challenge in protein science [6], and is the aim of some DMS studies [7, 8, 9, 10]. However, assaying molecular function, such as binding to a ligand, is a necessary and insufficient measure of stability, in that most proteins must be folded to function, but do not necessarily function if folded. In addition, high-throughput techniques, such as proteolysis assays [11], do not measure free energy, but measure scores that are correlated with stability. Similarly, scores from high-throughput binding assays do not measure binding energy in physical units, and do not distinguish whether changes seen in variants are due to changes in the overall fold stability or stability of the binding interface.

While high-throughput assays often confound function and stability, these can be separated with a thermodynamic approach. Thermodynamic approaches have been at the heart of biophysical models applied to data to quantify the evolution of regulatory sequences [12, 13, 14, 15], and proteins [16, 17, 18]. In the context of proteins, there are typically a few relevant conformational states, and the kinetics are fast enough to reach thermal equilibrium, with a free energy determining the probability of each state. At a minimum, a protein has folded and unfolded states, and other states may be due to binding, mis-folding, or some other conformational changes. Two-state models have been important in understanding observed patterns of substitutions in protein evolution [19, 20, 21], and in general, the ensemble of protein conformations generates epistasis that makes protein evolution difficult to predict [22]. A powerful simplification is to approximate the total energy by a sum over site-specific energies (additivity), which has been observed in most changes to fold stability [23, 24]. However, even with additivity in energy, the probability of a protein being in a particular state is non-linear with respect to energy and therefore epistatic with regard to sequence.

In this work, we infer a thermodynamic model that separates folding and stability in a small bacterial protein, protein G domain B1 (GB1), a model system of folding and stability, where a recent high-throughput assay of functional binding to an immunoglobulin fragment (IgG-Fc) described the epistasis between nearly all pairs of residues [10]. We infer a thermodynamic model with two states, bound, and unbound, and another model with three states: bound-folded, unbound-folded and unfolded. The approximation of additivity in energy allows us to separate how mutations destabilize the binding interface and how they destabilize the overall fold. We validate these approximations by predicting independently measured changes in fold stability. We describe the folding and stability landscape of the protein, identify which sites contribute most to binding, and explain much of the observed epistasis without assuming any energetic interactions.

Results

In vitro selection of protein variants

Olson et al. [10] mutagenized GB1 to create a library of protein variants which contained all single amino acid substitutions (1045 variants) and nearly all double substitutions (536k variants) of a reference or wild-type sequence. The library was sequenced before and after an *in vitro* selection assay, and the fraction of bound protein to IgG-Fc for a variant with sequence σ is $p'(\sigma) = \frac{n_1(\sigma)}{n_0(\sigma)r}$, where $n_0(\sigma)$ and $n_1(\sigma)$ are the sequence counts before and after selection, and r is a global factor that accounts for systematic differences between initial and final sequencing (see Methods for a maximum likelihood derivation of p'). For convenience, we define *fitness* as the logarithm of the binding fraction normalized by the wild-type σ^W

$$f(\sigma) = \log \left(\frac{n_1(\sigma) n_0(\sigma^W)}{n_0(\sigma) n_1(\sigma^W)} \right), \quad (1)$$

as an analogy to the growth rate of an exponentially growing population, although we do not imply that this is the (relative) growth rate of an organism with this variant.

With nearly every possible double substitution it is possible to study interactions between sites, or epistasis. We define pairwise epistasis in fitness as the difference between the fitness of the double mutants relative to the wild-type and the expectation of additivity, i.e., the sum of the fitness of two single mutants:

$$J_{ij}^{ab} = f(\sigma_{/(i,a)/(j,b)}^W) - f(\sigma_{/(i,a)}^W) - f(\sigma_{/(j,b)}^W). \quad (2)$$

where $/(i, a)$ and $/(j, b)$ indicate substitutions at positions i, j with amino acids a, b .

While changes in fitness across all single and double mutants show where a protein is sensitive to binding, such changes are not informative of whether mutations are destabilizing the binding interface or the overall fold, as changes in either one influence the fraction of bound protein. A thermodynamic model is necessary to separate these effects.

Thermodynamic models

Proteins fold into complicated structures and interact with other molecules depending on the free energy of their different states or conformations. Under natural conditions, protein states reach thermodynamic equilibrium very quickly and the Boltzmann distribution relates the probability of state i to the free energy E_i : $p_i(\sigma) = \frac{1}{Z} e^{-E_i(\sigma)}$, where $E_i(\sigma)$ are in dimensionless units and Z is the normalization factor over states [25]. For a two state bound/unbound model, the fraction of bound protein is $\frac{1}{1+e^{E(\sigma)}}$, with energy $E(\sigma)$. In order to separate binding and stability, we define three states: unfolded and unbound, folded and unbound, and folded and bound, and therefore the fraction of bound protein is

$$p(\sigma) = \frac{e^{-E_f(\sigma)-E_b(\sigma)}}{1 + e^{-E_f(\sigma)} + e^{-E_f(\sigma)-E_b(\sigma)}} = \frac{1}{1 + e^{E_b(\sigma)}(1 + e^{E_f(\sigma)})} \quad (3)$$

with folding energy $E_f(\sigma)$ and binding energy $E_b(\sigma)$. The folding energy is relative to the unfolded state, whereas the binding energy is relative to the folded-unbound state, up to a constant that depends on the concentration of ligand (the chemical potential). Importantly, this binding energy measures only the destabilization of the binding interface, and is distinct from dissociation constants that are related to our model by $K_d \propto e^{E_b}(1 + e^{E_f})$ (neglecting the chemical potential). Intuitively, low binding and folding energy leads

to large p , and the shaded areas in Fig. 1 show regions in energy space where each label indicates the most likely state.

Given an experimentally measured p of a single variant, there are many values E_b and E_f that match p , and it is not possible to identify these energies, as shown by the contour lines of equal p in Fig. 1. However, with the approximation of additivity in energy over sites, it is possible to combine information from many sequences to estimate energies. Additivity means that the energy is a sum over energies specific to each substitution $\epsilon(i, a)$:

$$E_f(\sigma) = \epsilon_f^W + \sum_i \epsilon_f(i, \sigma_i) \quad (4)$$

$$E_b(\sigma) = \epsilon_b^W + \sum_i \epsilon_b(i, \sigma_i) \quad (5)$$

where subscripts f and b indicate folding and binding respectively, σ_i is the amino acid at position i , and $\epsilon(i, \sigma_i^W) = 0$ so that the wild-type energy is ϵ^W . While additivity has been observed in many experimental measurements of changes in fold stability [23, 24], it is a local approximation that is likely to be violated for highly mutated sequences.

To illustrate how multiple data points constrain this non-linear model, consider a hypothetical quartet of sequences and their measured binding fraction p : the wild-type, two sequences with single substitutions, and a sequence with both of those substitutions. The lines in Fig. 1 are the energy coordinates consistent with the given p , and the dashed lines are the additive energies that connect the wild-type (red line) to the single mutants (black lines), and to the double mutant (blue line). The parameters are not constrained given a wild-type p and single mutant p , as a rectangles can be placed anywhere between two lines as long as the opposing corners land on them. However, when considering all four sequences the largest rectangle must have lengths that are the sum of the smaller rectangle lengths due to additivity, and the non-linearity of the curves constrains the parameters (additive energies) that can fit the data, with more data providing more constraints.

We use all sequences and associated counts in a maximum a likelihood framework to infer all additive and wild-type folding and binding energies, converted to kcal/mol (see Methods). For comparison, we also infer energies of the two state model. In Methods, we modify the likelihood to account for non-specific background binding, and describe a procedure to overcome local optima via bootstrapping.

Inferred energy landscape

We compare the inferred additive folding energies to independent low-throughput measurements of 81 single substitutions in Fig. 2A (collected from different sources in [10]). The three state model (bound/unbound/unfolded) accurately predicts ϵ_f in physical units with an root mean squared error of 0.39 kcal/mol and a correlation of $\rho = 0.91$, which is better than computational methods (~ 0.6 to ~ 0.7) and close to the amount of correlation between replicates of low-throughput methods (~ 0.86) [26]. Six variants with 2-6 mutations are also predicted (Fig. 2A red) with comparable accuracy. However, 2 highly stable variants (G β 1-c3b4 with 7 mutations, and M2 with 4, not shown) are underestimated by 2.1 and 5.3 kcal/M respectively, suggesting the presence of significant synergistic epistasis in the folding energy for these variants.

The two state model (bound/unbound) fits the data similarly well to the three state model, with a correlation between predicted fitness $\hat{f}(\sigma) = \log(p(\sigma)/p(\sigma^W))$ and measured fitness of 96.4% and 97.1% for two and three state models respectively (see Fig. S1). However, the additive energies inferred by the two

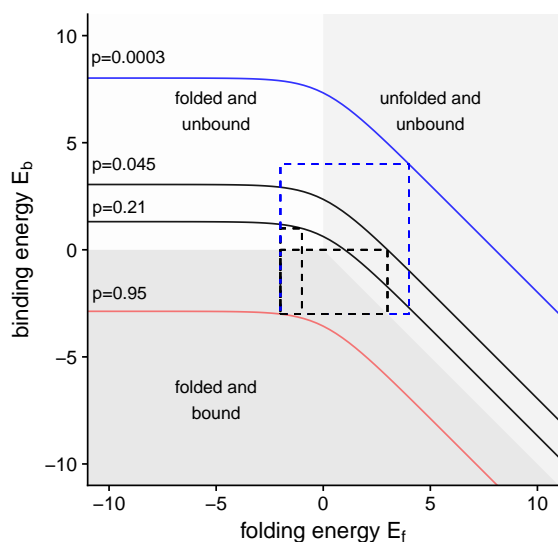


Figure 1: Thermodynamic model of three protein states: unfolded and unbound, folded and unbound, and folded and bound, described by eq. 3. Shaded areas correspond to regions in energy space where the labeled state is dominant. Given sequences and binding fractions p , the non-linear Boltzmann form (eq. 3) imposes constraints on the possible parameters (additive energies). Solid lines are the energies compatible with p for four hypothetical sequences: wild-type (red), two single mutants (black) and a double mutant (blue). Dashed lines represent additive energies, and connect the wild-type to the single mutants (black) and the double mutant (blue), which has lengths equal to the sum of additive energies.

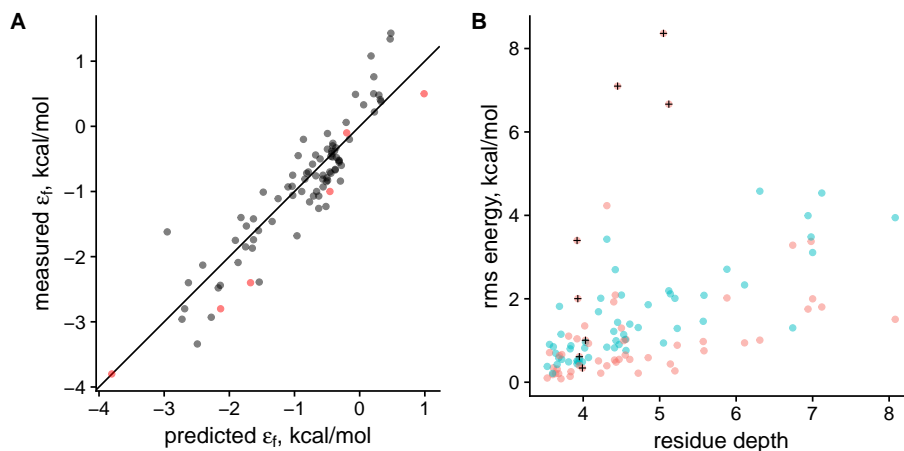


Figure 2: A) Accurate prediction of changes in folding energy ϵ_f (eq. 4, commonly referred to as $\Delta\Delta G$) by fitting a three state thermodynamic model to deep mutational scanning data. Predicted energies have a root mean square error of 0.39 kcal/mol and $\rho = 0.91$ compared to independent measurements of ϵ_f for 81 single substitutions [10]. Six variants with 2-6 mutations are shown in red. The line has a slope of unity. B) Folding energies (teal) have a stronger relation to residue depth than binding energies (red). Root mean square energy changes at each position are shown, and a plus sign indicates sites at the protein-protein interface [27, 28]).

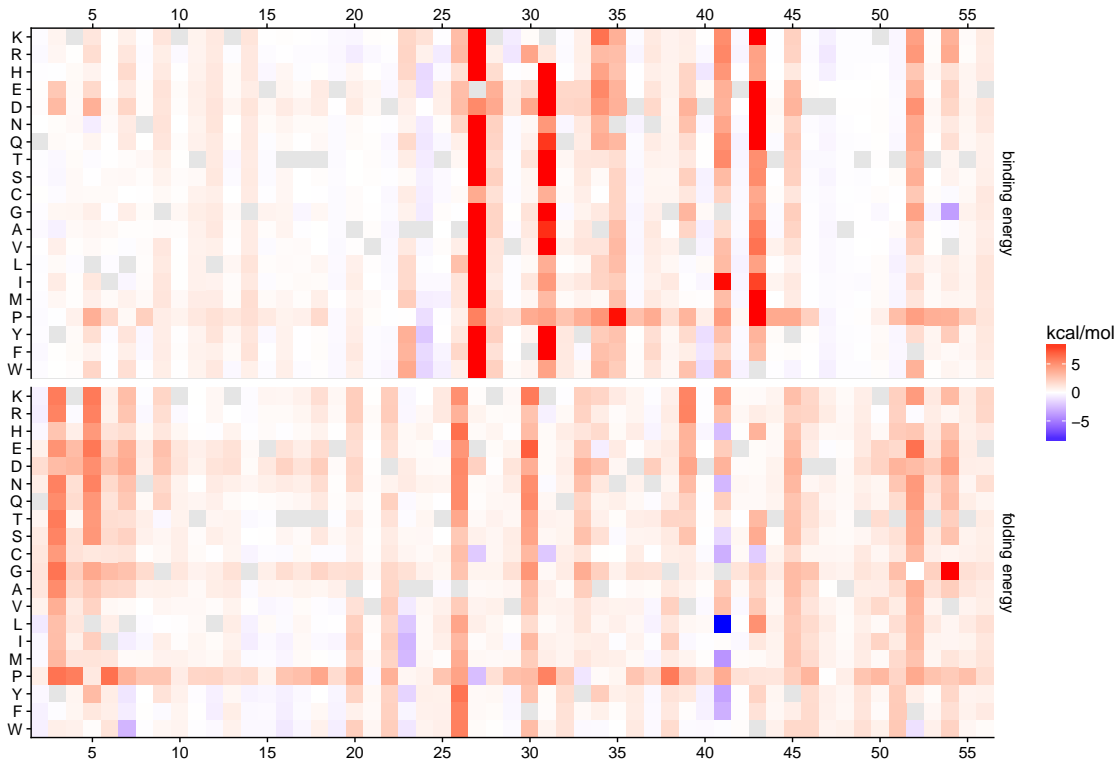


Figure 3: Inferred additive binding ϵ_b and folding ϵ_f energies show strikingly different patterns. Three of the binding sites (27, 31, 43) have strong effects on binding. Many substitutions at positions 23 and 41 are beneficial for folding and deleterious for binding, although overall substitutions are uncorrelated.

state model have no relation to the independently measured ϵ_f (Fig. S2). Clearly a three state model is necessary to predict folding energy, and has the added benefit of estimating binding energy.

To assess how much sampling noise influences our results, we calculate 95% confidence intervals of ϵ_f and ϵ_b from the bootstrapped estimates (Fig. S3), and find that they are very narrow compared to the range of effect sizes for most of the 2092 energy parameters. Examining ϵ_f and ϵ_b across sites and amino acids (Fig. 3) reveals a detailed picture of how folding and binding are sensitive to substitutions. The energies have striking differences in their patterns, and ϵ_f and ϵ_b are uncorrelated (Fig. 4A, $\rho = 0.03$, $p_{value} = .28$). Some substitutions have strong antagonistic effects, such as at positions 23 and 41, neither of which are at the binding interface. The substitutions 41L and 54G have particularly strong antagonism, although the double mutant is known to be strongly epistatic, and there may be systematic errors in these parameters from effects not captured by our model. With relatively few exceptions, amino acid substitutions in GB1 do not produce trade-offs between binding and fold stability.

The energy landscape of a protein is determined by its structure, so we expect that the inferred energies are related to structural features. Both ϵ_f and ϵ_b correlate with residue depth (Fig. 2B), and ϵ_b has a weaker relation to depth, except for a few sensitive shallow residues. The three most sensitive sites to binding are at the interface of the two proteins [27, 28] (plus signs in Fig. 2B), but many other sites at the interface are not sensitive.

A top down view of folding vs. binding energy of single and double mutants depicts how the variants fall into each of the three states. In this phenotypic space, the wild-type is better than most of the observed sequences, and in terms of binding fraction, it is in the 72nd and 85th percentile of the single and double

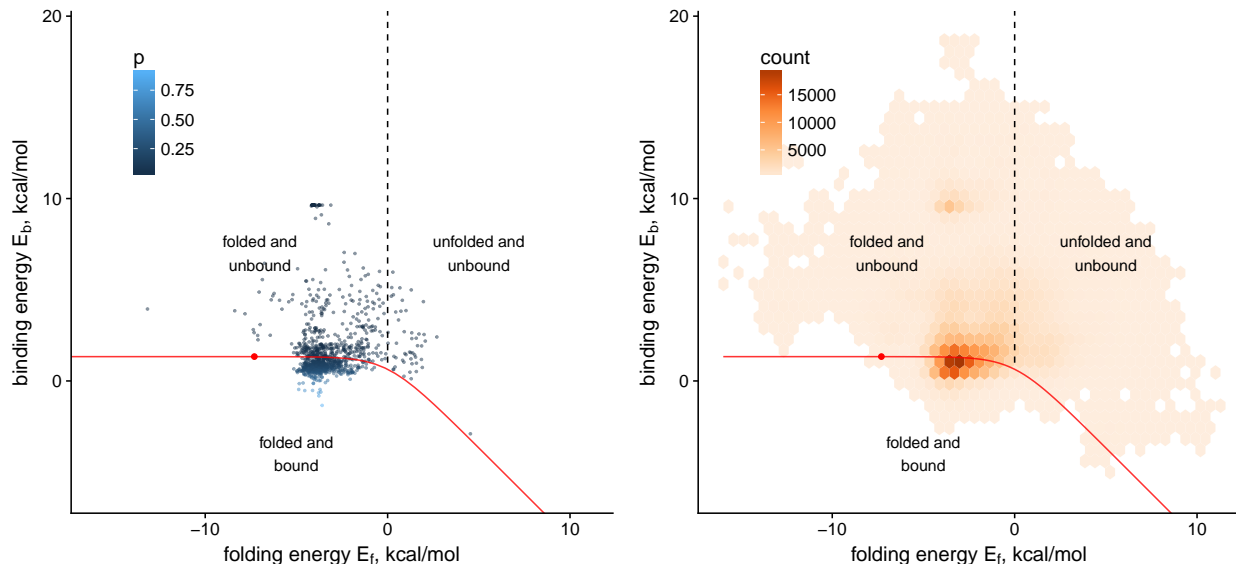


Figure 4: Folding vs. binding energy for single (A) and double (B) mutants. Red dot is the wild-type energy, the red line is where binding fraction is the same as wild-type $p = p^W$, and below the red line variants have $p > p^W$. The three equilibrium states are labeled, with $E_f = 0$ demarcating the folded and unfolded states.

substitutions respectively. Most variants fall in the region of excess stability ($E_f \ll 0$), whereas binding energies are distributed around the wild-type, implying that binding fraction is more sensitive to changes in binding energy than folding energy for the majority of variants. This is consistent with the lack of correlation between additive energies from the two state model and independently measured folding energies (Fig. S2), as well as the lack of correlation between changes in fitness and folding energies [10].

Patterns of epistasis

While the energies in our models are non-epistatic, the binding fraction and fitness are epistatic due to the non-linearity between binding fraction and energy (eq. 3), and our inferred pairwise epistasis \hat{J}_{ij}^{ab} , analogous to eq. 2, can be compared to the observed epistasis. We filter out non-biological epistasis due to experimental limits on measured fitness, i.e., non-specific background binding (see Methods), and average over amino acids in each pair of sites. The predictions from the three-state model reproduces the biological epistasis better than the two-state model, which vastly underestimates the magnitude of epistasis across the protein (Fig. 5). Notably, the three state model predicts much of the negative epistasis, but misses clusters of positive epistasis.

To quantify these deviations, the difference between the predicted and observed epistasis can be normalized by the noise in the observed epistasis, $z_{ij} = \frac{\hat{J}_{ij} - J_{ij}}{\sqrt{v_{J_{ij}}}}$ (see Methods). The clusters of positive epistasis are more clearly visible after filtering out all but the most underestimated epistasis (bottom 5% of z_{ij} , Fig. S4). As noted in [10], the residues in these positions had correlated conformational dynamics in NMR and molecular dynamics studies (positions 7, 9, 11, 12, 14, 16, 33, 37, 38, 40, 54, 56, [29, 30, 31]). This suggests that this unexplained epistasis is due to systematic errors not accounted for in the model, such as epistasis in energy or some alternative conformations, and therefore large prediction errors can identify sites that should be studied in more detail.

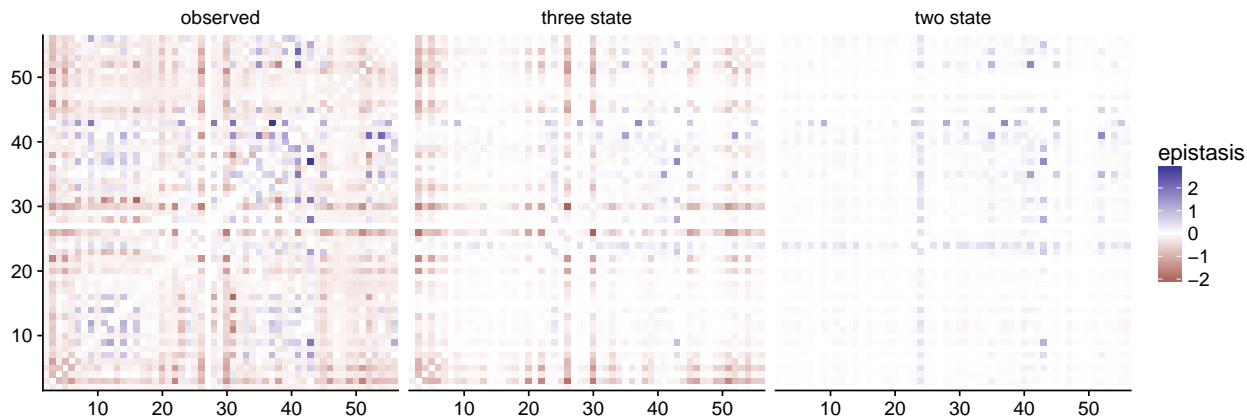


Figure 5: Patterns of pairwise epistasis observed in the data and predicted by the three state and two state thermodynamic models. Shown are observed pairwise fitness epistasis (eq. 2), and inferred epistasis from the three state model and the two state model. A network of residues that undergo correlated conformational dynamics (positions 7, 9, 11, 12, 14, 16, 33, 37, 38, 40, 54, 56) have significant observed positive epistasis that the thermodynamic models fail to estimate. Epistasis is averaged for each pair of sites over the relevant amino acid substitutions. We filter out non-biological epistasis that is a consequence of the experimental limits on measured fitness due to non-specific background binding (see Methods).

We also made predictions for a follow up study by Wu et al. [32], which targeted 4 highly epistatic sites in GB1, and assayed all combinations of mutations, i.e. 20^4 variants. Most of the mutants with 3 or 4 mutations have very weak binding, and the fitness predictions from the model trained on the Olson et. al data can roughly predict their functionality (Fig. S5). Our model predicts functional quadruple mutants with a true positive rate of 86% and a true negative rate of 95% (defining functional as $f > -2.5$, Tab. S1). At the same time, the fitness is underestimated for many variants much more than expected from measurement variability (Fig. S6), suggesting that, in this more mutated data, some unaccounted for epistasis is restoring binding or stability for approximately 20% of variants.

Discussion

We have shown how with a few biophysical assumptions, i.e., a small number of thermodynamic states and additivity of energy, are sufficient to extract a detailed folding and binding energy landscape of a protein. Many DMS studies use *in vitro* and *in vivo* selection assays, and quantify the results with enrichment ratios, similar to fitness in eq. 1. Most of these studies focus on single substitutions from a wild-type, however fitness changes of single substitutions confound changes in stability and binding. We have shown how combining information from multiple sequences with many mutations provide the constraints to separate these phenotypes in a thermodynamic model, and therefore highly mutagenized sequence-function experiments can provide a rich description of a protein’s energy landscape.

The inferred energies from the three state model very accurately predict the independent low-throughput measurements, and show that it is feasible to infer folding and binding energy in physical units accurately from simple high-throughput functional assays. Several DMS studies have indirectly measured stability. Araya et al. [7] applied a metric, based on the rescue effect of double mutations, to identify stabilizing mutations, and Rocklin et al. [11] used proteolysis assays that correlate with stability. Olson et al. [10] extracted stability measures from this dataset by searching for single mutation fitness changes in different genetic backgrounds

that correlated with the literature set of stability measurements. Further refinements were developed with clustering methods that use structural information and physiochemical properties [33]. However, these ad-hoc methods can suffer from over-fitting and require extraneous knowledge to work effectively. In contrast, the thermodynamic model directly infers stability in physical units and does not require any benchmark stability measurements or structural information.

Our method also infers the binding energies that are marginal to the folded–unbound state and measure the destabilization of the binding interface. In contrast, dissociation constants, as measured by titration curves, do not account for differences in fold stability. The recently developed tite-seq method [34] infers a saturation constant to account for sequence dependent differences in stability and expression, but does not compensate for stability effects in the dissociation constant itself.

We have shown that the three state model shows good agreement with patterns of epistasis, and deviations from our model identify a network of residues that have correlated conformational dynamics. Since the deviations and measurement noise itself can be rather large, sign epistasis, path accessibility, and other geometric features of the inferred genotype-phenotype map are likely to be distorted. It is possible that more complex models, such energetic interaction terms or more conformational states, can describe the remaining epistasis in double mutants and in variants with more than two mutations. The three state model works well for the relatively small GB1, but larger proteins may need additional states, such as mis-folded conformations, to accurately model their properties.

Inferred energy landscapes from DMS may also be useful in understanding protein structure. Inferred energy parameters may be useful for calibrating potential functions used in structure prediction [35]. Refined thermodynamic models with pairwise epistatic energy may be able to infer protein contacts directly, similar to how multiple sequence alignments of homologous proteins can infer contacts [36], providing a way to predict structure from DMS studies. Thermodynamic models coupled with DMS also provide a way to study intrinsically disordered proteins, which fold and bind simultaneously, but have no persistent structure while unbound [37]. Since many conformations can correspond to these states, free energy differences are a natural way to quantify the properties of disordered proteins.

While we have inferred a detailed genotype-phenotype map of GB1, yet we do not know the consequences for evolution, which depend on how the binding fraction affects the organismal fitness. Manhart and Morozov [38] explored the evolutionary dynamics of a fitness function that is a linear combination of the three protein states. This leads to an evolutionary coupling between binding and folding, where selection on folding can drive changes in binding, and vice versa. With appropriate data it may be possible to infer selection coefficients associated with each state, as well as evolutionary trajectories in energy space, from multiple sequence alignments.

Methods

Poisson likelihood for an *in vitro* selection assay

In an *in vitro* selection assay with one round, the library of protein variants is sequenced before and after binding, and therefore the count or multiplicity of each sequence carries information on the binding. For each variant σ , with initial and final counts n_0 and n_1 , we define a Poisson log-likelihood with intensity $\lambda_0 = N_0$ and $\lambda_1 = N_0 p r$, where p represents the fraction of bound protein and r is the systematic difference between

initial and final sequencing. We omit the dependence on σ for brevity (note that r does not depend on σ). The per variant joint likelihood over the two time points is

$$LL = -N_0(1 + pr) + n_0 \log(N_0) + n_1 \log(N_0 pr), \quad (6)$$

omitting terms that don't depend on parameters. This has a nuisance parameter N_0 per sequence, which has an ML estimate, given the other parameters

$$N_0^* = \frac{n_0 + n_1}{1 + pr}$$

Plugging it into the likelihood and dropping terms which don't depend on the parameters results in

$$LL = -(n_0 + n_1) \log(1 + pr) + n_1 \log(pr). \quad (7)$$

The maximum likelihood estimate of binding fraction is $p' = \frac{n_1}{n_0 r}$. Since some of the counts can be very small, we add a pseudo-count of $\frac{1}{2}$ to n_0 and n_1 to slightly regularize the estimate.

Thermodynamic model inference

We use the likelihood in eq. 7, and parameterize p as a thermodynamic model following the Boltzmann distribution. We modify p to account for non-specific background binding p_0 :

$$p(\sigma) = \frac{1}{1 + e^{E_b(\sigma)}(1 + e^{E_f(\sigma)})} (1 - p_0) + p_0, \quad (8)$$

and the energies have an additive relation to sequence defined by eqs. 45. The total likelihood is the sum of the per variant likelihoods $\mathbf{LL} = \sum_{\sigma} LL(\sigma)$.

This log-likelihood is non-convex, and is optimized using the NLOpt library [39], which implements the method of moving asymptotes algorithm [40], and uses the log-likelihood gradients with respect to r , p_0 , and the energies. The initial parameters were $r = 1$, $p_0 = 0.01$, and all energies set to zero. r and p_0 were reparameterized as $e^{r'}$ and $e^{p'_0}$ inside the optimization function, so that the original parameters are non-negative. In the optimization algorithm, upper and lower bounds on ε are set to limit very small gradients which stop the optimization prematurely. The value of ± 15 was chosen by optimizing with different bounds, ± 10 , ± 15 , ± 20 , and ± 25 , and choosing the result with the highest likelihood. Dimensionless energies are converted to kcal/mol with $T = 297$, and therefore the bounds are ± 8.85 kcal/mol.

Bootstrap

Since the optimization algorithm can get stuck in local optima, we use a bootstrap restarting procedure to overcome local optima related to sampling noise [41], and to generate a bootstrap distribution of parameters to quantify their uncertainty due to sampling noise. The maximum likelihood parameters from the fit described above, θ , are the initial parameters in an iterative procedure that alternates optimizing on the original and bootstrapped data.

Each iteration consists of: 1) creation of bootstrapped data with counts drawn from a Poisson distribution with means n_0 and n_1 . 2) Searching for the maximum likelihood parameters θ' on the bootstrapped data with initial parameters θ . 3) Searching for the maximum likelihood parameters θ'' on the original data with

initial parameters θ' . 4) If the likelihood is no better than the best optimization within a small threshold $LL(\theta'') \leq LL(\theta) + \eta$ ($\eta = 0.0001$), then add the bootstrapped parameters θ' to a list. 5) If the likelihood is better than the previous best $LL(\theta'') > LL(\theta) + \eta$, then update the best parameters, $\theta \leftarrow \theta''$, and delete the list of bootstrapped parameters. 6) terminate the procedure once 100 bootstraps have been accumulated in the list.

Pairwise epistasis

A minimal amount of non-specific background binding, p_0 , imposes a lower bound on measured binding fraction in the experiment, estimated to be $f_0 = \log(p_0/p(\sigma^W)) = -5.69$ by our three state model. This threshold effect produces large amounts of non-biological positive pairwise epistasis, e.g. when the double mutant has the same level of binding as one of the single mutants at the background level. Therefore, the data shown in Fig. 5 excludes \hat{J}_{ij}^{ab} with sequences near this threshold, i.e., $\min\left(f(\sigma_{(i,a)/(j,b)}^W), f(\sigma_{(i,a)}^W), f(\sigma_{(j,b)}^W)\right) < -4.5$.

Sample variance of fitness and epistasis

Since estimated fitness is asymptotically Gaussian, the sample variance of fitness is equal to the curvature of the log-likelihood surface. Replacing p' with $e^{f'}$ in eq. 7, the asymptotic variance of f' is $-\left(\frac{\partial^2 LL}{\partial f'^2}\right)^{-1}$. The variance of the fitness estimate, as defined in eq. 1 is the sum of the focal and wild-type variances

$$v_f(\sigma) = \frac{n_0(\sigma) + n_1(\sigma)}{n_0(\sigma)n_1(\sigma)} + \frac{n_0(\sigma^W) + n_1(\sigma^W)}{n_0(\sigma^W)n_1(\sigma^W)}, \quad (9)$$

and the variance in epistasis is the sum of the single and double mutant variances

$$v_{J_{ij}^{ab}} = v_f(\sigma_{(i,a)/(j,b)}^W) + v_f(\sigma_{(i,a)}^W) + v_f(\sigma_{(j,b)}^W),$$

The variance is then averaged over amino acids a, b for each position i, j .

References

- [1] Douglas M Fowler and Stanley Fields. Deep mutational scanning: a new style of protein science. *Nature Methods*, 11(8):801–807, 2014.
- [2] Emily E Wrenbeck, Matthew S Faber, and Timothy A Whitehead. Deep sequencing methods for protein engineering and design. *Current Opinion in Structural Biology*, 45:36–44, August 2017.
- [3] Jakub Otwinowski and Joshua B Plotkin. Inferring fitness landscapes by regression produces biased estimates of epistasis. *Proceedings of the National Academy of Sciences of the United States of America*, 111:E2301–9, May 2014.
- [4] Louis du Plessis, Gabriel E. Leventhal, and Sebastian Bonhoeffer. How good are statistical models at approximating complex fitness landscapes. *Mol Biol Evol*, page msw097, May 2016.
- [5] Shimon Bershtein, Adrian WR Serohijos, and Eugene I Shakhnovich. Bridging the physical scales in evolutionary biology: from protein sequence space to fitness of organisms and populations. *Current Opinion in Structural Biology*, 42:31–40, February 2017.

- [6] Thomas J Magliery, Jason J Lavinder, and Brandon J Sullivan. Protein stability by number: high-throughput and statistical approaches to one of protein science’s most difficult problems. *Current Opinion in Chemical Biology*, 15(3):443–451, June 2011.
- [7] C. L. Araya, D. M. Fowler, W. Chen, I. Muniez, J. W. Kelly, and S. Fields. A fundamental protein property, thermodynamic stability, revealed solely from large-scale measurements of protein function. *Proceedings of the National Academy of Sciences*, 109(42), 2012.
- [8] Michael W. Traxlmayr, Christoph Hasenhindl, Matthias Hackl, Gerhard Stadlmayr, Jakub D. Rybka, Nicole Borth, Johannes Grillari, Florian R uker, and Christian Obinger. Construction of a Stability Landscape of the CH3 Domain of Human IgG1 by Combining Directed Evolution with High Throughput Sequencing. *Journal of Molecular Biology*, 423(3):397–412, October 2012.
- [9] Ikjin Kim, Christina R. Miller, David L. Young, and Stanley Fields. High-throughput Analysis of in vivo Protein Stability. *Molecular & Cellular Proteomics*, page mcp.O113.031708, 2013.
- [10] C. Anders Olson, Nicholas C. Wu, and Ren Sun. A Comprehensive Biophysical Description of Pairwise Epistasis throughout an Entire Protein Domain. *Current Biology*, 24(22):2643–2651, 2014.
- [11] Gabriel J. Rocklin, Tamuka M. Chidyausiku, Inna Goreschnik, Alex Ford, Scott Houliston, Alexander Lemak, Lauren Carter, Rashmi Ravichandran, Vikram K. Mulligan, Aaron Chevalier, Cheryl H. Arrow-smith, and David Baker. Global analysis of protein folding using massively parallel design, synthesis, and testing. *Science*, 357(6347):168–175, July 2017.
- [12] Ville Mustonen and Michael L assig. Evolutionary population genetics of promoters: Predicting binding sites and functional phylogenies. *PNAS*, 102(44):15936–15941, November 2005.
- [13] Ville Mustonen, Justin Kinney, Curtis G Callan, and Michael L assig. Energy-dependent fitness: a quantitative model for the evolution of yeast transcription factor binding sites. *Proceedings of the National Academy of Sciences of the United States of America*, 105(34):12376–81, August 2008.
- [14] Justin B Kinney, Anand Murugan, Curtis G Callan, and Edward C Cox. Using deep sequencing to characterize the biophysical mechanism of a transcriptional regulatory sequence. *Proceedings of the National Academy of Sciences of the United States of America*, 107(20):9158–63, May 2010.
- [15] Mato Lagator, Tiago Paix o, Nicholas H. Barton, Jonathan P. Bollback, and C alin C. Guet. On the mechanistic nature of epistasis in a canonical cis-regulatory element. *eLife Sciences*, 6:e25192, May 2017.
- [16] Jesse D. Bloom, Jonathan J. Silberg, Claus O. Wilke, D. Allan Drummond, Christoph Adami, Frances H. Arnold, and Alan R. Fersht. Thermodynamic Prediction of Protein Neutrality. *Proceedings of the National Academy of Sciences of the United States of America*, 102(3):606–611, 2005.
- [17] C. Scott Wylie and Eugene I. Shakhnovich. A biophysical protein folding model accounts for most mutational fitness effects in viruses. *PNAS*, 108(24):9916–9921, June 2011.
- [18] Julian Echave and Claus O. Wilke. Biophysical Models of Protein Evolution: Understanding the Patterns of Evolutionary Sequence Divergence. *Annual Review of Biophysics*, 46(1):85–103, 2017.
- [19] Tyler N. Starr and Joseph W. Thornton. Epistasis in protein evolution. *Protein Science*, 25(7):1204–1218, July 2016.

- [20] Ugo Bastolla, Yves Dehouck, and Julian Echave. What evolution tells us about protein physics, and protein physics tells us about evolution. *Current Opinion in Structural Biology*, 42:59–66, February 2017.
- [21] David a Liberles, Sarah a Teichmann, Ivet Bahar, Ugo Bastolla, Jesse Bloom, Erich Bornberg-Bauer, Lucy J Colwell, a P Jason de Koning, Nikolay V Dokholyan, Julian Echave, Arne Elofsson, Dietlind L Gerloff, Richard a Goldstein, Johan a Grahnen, Mark T Holder, Clemens Lakner, Nicholas Lartillot, Simon C Lovell, Gavin Naylor, Tina Perica, David D Pollock, Tal Pupko, Lynne Regan, Andrew Roger, Nimrod Rubinstein, Eugene Shakhnovich, Kimmen Sjölander, Shamil Sunyaev, Ashley I Teufel, Jeffrey L Thorne, Joseph W Thornton, Daniel M Weinreich, and Simon Whelan. The interface of protein structure, protein biophysics, and molecular evolution. *Protein science : a publication of the Protein Society*, 21(6):769–85, June 2012.
- [22] Zachary R. Sailer and Michael J. Harms. Molecular ensembles make evolution unpredictable. *PNAS*, page 201711927, October 2017.
- [23] J. A. Wells. Additivity of mutational effects in proteins. *Biochemistry*, 29(37):8509–8517, September 1990.
- [24] W. S. Sandberg and T. C. Terwilliger. Engineering multiple properties of a protein by combinatorial mutagenesis. *PNAS*, 90(18):8367–8371, September 1993.
- [25] Rob Phillips, Jane Kondev, Julie Theriot, and Hernan Garcia. *Physical Biology of the Cell, Second Edition*. Garland Science, October 2012.
- [26] Vladimir Potapov, Mati Cohen, and Gideon Schreiber. Assessing computational methods for predicting protein stability upon mutation: good on average but not in the details. *Protein Eng Des Sel*, 22(9):553–560, September 2009.
- [27] A. Elisabeth Sauer-Eriksson, Gerard J Kleywegt, Mathias Uhlen, and T. Alwyn Jones. Crystal structure of the C2 fragment of streptococcal protein G in complex with the Fc domain of human IgG. *Structure*, 3(3):265–278, March 1995.
- [28] David J. Sloan and Homme W. Hellinga. Dissection of the protein G B1 domain binding site for human IgG Fc fragment. *Protein Science*, 8(8):1643–1648, January 1999.
- [29] G. Marius Clore and Charles D. Schwieters. Amplitudes of protein backbone dynamics and correlated motions in a small alpha/beta protein: correspondence of dipolar coupling and heteronuclear relaxation measurements. *Biochemistry*, 43(33):10678–10691, August 2004.
- [30] Oliver F. Lange, Helmut Grubmüller, and Bert L. de Groot. Molecular dynamics simulations of protein G challenge NMR-derived correlated backbone motions. *Angew. Chem. Int. Ed. Engl.*, 44(22):3394–3399, May 2005.
- [31] Phineus R. L. Markwick, Guillaume Bouvignies, and Martin Blackledge. Exploring multiple timescale motions in protein GB3 using accelerated molecular dynamics and NMR spectroscopy. *J. Am. Chem. Soc.*, 129(15):4724–4730, April 2007.
- [32] Nicholas C. Wu, Lei Dai, C. Anders Olson, James O. Lloyd-Smith, and Ren Sun. Adaptation in protein fitness landscapes is facilitated by indirect paths. *eLife*, 5:e16965, July 2016.

- [33] Nicholas C. Wu, C. Anders Olson, and Ren Sun. High-throughput identification of protein mutant stability computed from a double mutant fitness landscape. *Protein Science*, pages n/a–n/a, December 2015.
- [34] Rhys M. Adams, Thierry Mora, Aleksandra M. Walczak, and Justin B. Kinney. Measuring the sequence-affinity landscape of antibodies with massively parallel titration curves. *eLife Sciences*, 5:e23156, December 2016.
- [35] Jooyoung Lee, Peter L. Freddolino, and Yang Zhang. Ab Initio Protein Structure Prediction. In *From Protein Structure to Function with Bioinformatics*, pages 3–35. Springer, Dordrecht, 2017.
- [36] Faruck Morcos, Terence Hwa, JosÅ© N Onuchic, and Martin Weigt. Direct Coupling Analysis for Protein Contact Prediction. In Daisuke Kihara, editor, *Protein Structure Prediction*, volume 1137 of *Methods in Molecular Biology*, pages 55–70. Springer New York, New York, NY, 2014.
- [37] Peter E Wright and H Jane Dyson. Linking folding and binding. *Current Opinion in Structural Biology*, 19(1):31–38, February 2009.
- [38] Michael Manhart and Alexandre V. Morozov. Protein folding and binding can emerge as evolutionary spandrels through structural coupling. *PNAS*, 112(6):1797–1802, February 2015.
- [39] Steven G. Johnson. The NLOpt nonlinear-optimization package.
- [40] Krister Svanberg. A class of globally convergent optimization methods based on conservative convex separable approximations. *SIAM Journal on Optimization*, pages 555–573.
- [41] Simon N. Wood. Minimizing Model Fitting Objectives That Contain Spurious Local Minima by Bootstrap Restarting. *Biometrics*, 57(1):240–244, March 2001.

Supplemental Material

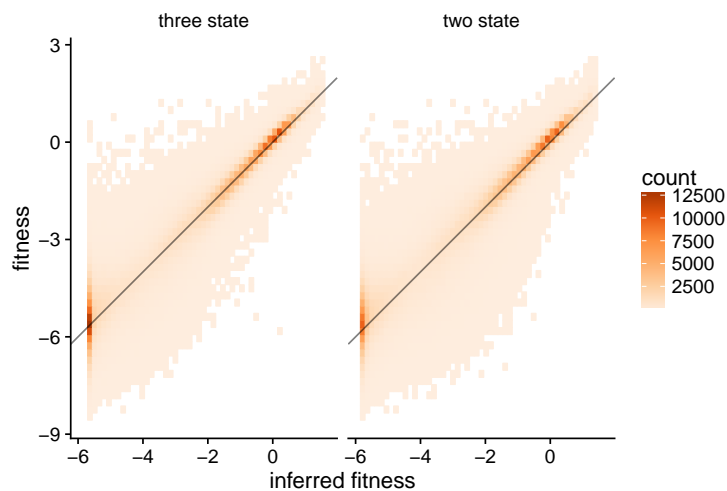


Figure S1: Inferred versus predicted fitness for two state model and three state model. Correlations are 96.4% and 97.1% respectively.

| d_h | n | ρ | TP | FP | TN | FN |
|-------|--------|--------|------|-----|--------|------|
| 1 | 76 | 0.95 | 39 | 1 | 29 | 7 |
| 2 | 2091 | 0.74 | 498 | 19 | 1342 | 232 |
| 3 | 26019 | 0.42 | 1596 | 158 | 21355 | 2910 |
| 4 | 121174 | 0.39 | 982 | 162 | 113984 | 6046 |

Table S1: Statistics for predictions on Wu et. al data. d_h : hamming distance from wild-type. n : number of variants. ρ : correlation coefficient weighted by $1/v_f$. TP, FP, TN, FN: True/false positives/negatives for whether the variant is functional ($f > -2.5$).

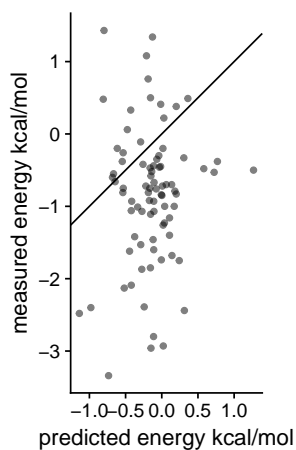


Figure S2: Additive energies from two state model do not predict changes in fold stability. Measured ϵ same as in fig. 2B. If variants have excess stability, the measured binding fraction would be mostly sensitive to binding, which would lead to energies unrelated to folding.

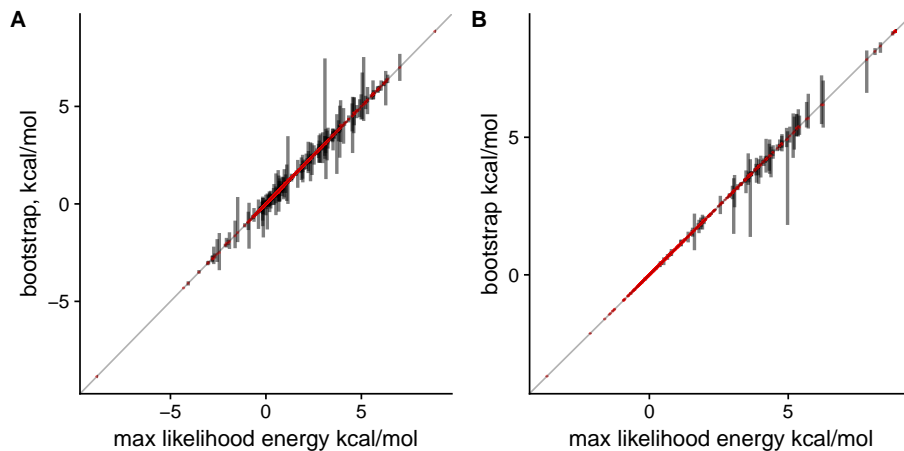


Figure S3: Bootstrapped parameters of the three state model, for the folding (A) and binding (B) energies. Red points denote the median value from the bootstrap, and the gray bars show the 95% confidence interval.

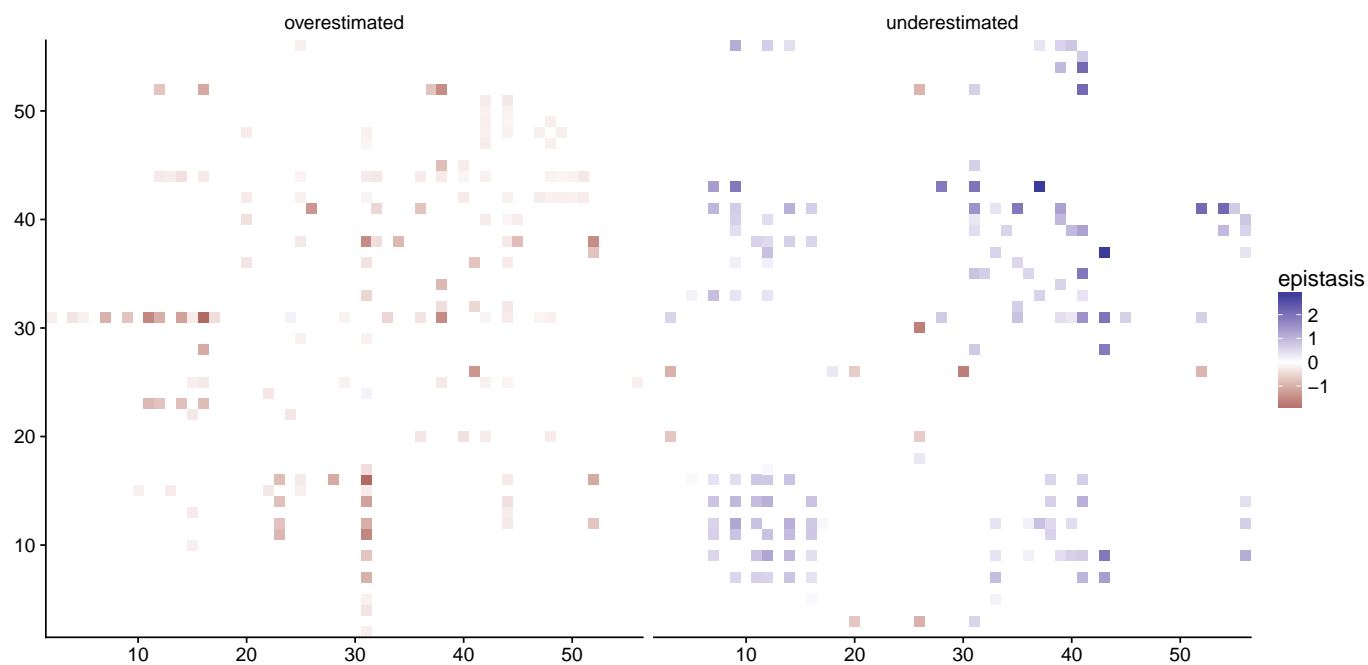


Figure S4: Observed epistasis J_{ij} (averaged over amino acids) which our model overestimates ($\hat{J}_{ij} \gg J_{ij}$) and underestimates ($\hat{J}_{ij} \ll J_{ij}$). Overestimated epistasis is the top 5% of z_{ij} and underestimated epistasis is the bottom 5%. Underestimated epistasis is largely positive and corresponds to the dynamically correlated residue network.

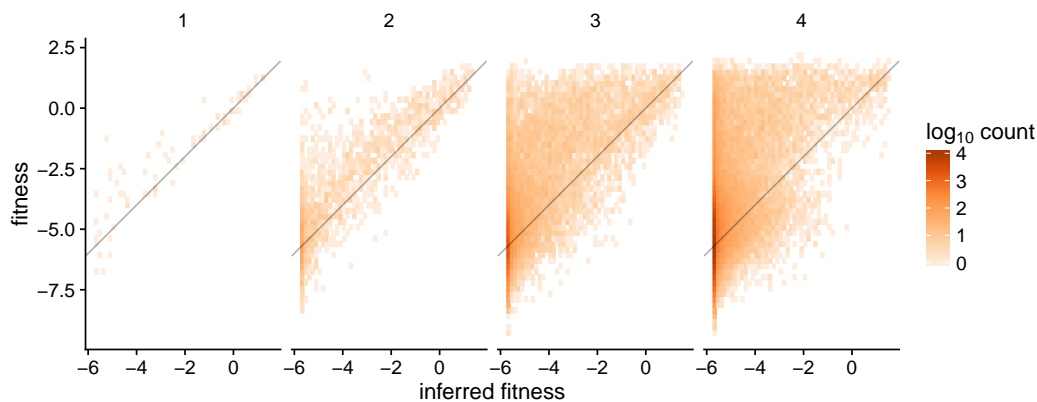


Figure S5: Fitness is less predictable in a follow-up study that targeted all combinations at four sites [32]. Panels show true and inferred fitness for 1 to 4 substitutions from wild-type. A substantial fraction of functional variants are underestimated, suggesting some unaccounted for epistasis in energy or conformational dynamics. See also Fig. S6 and Tab. S1.

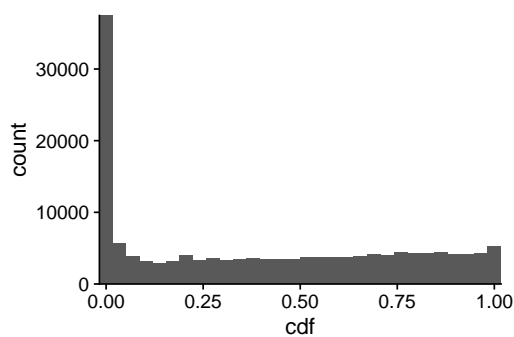


Figure S6: Around 20% of variants in Wu et al predictions have fitnesses underestimated more than expected from measurement variation. Shown is distribution of CDF $\left(\frac{\hat{f}(\sigma) - f(\sigma)}{\sqrt{v_f(\sigma)}}\right)$, where CDF is the cumulative distribution function of a standard normal distribution.